Frazil ice formation in an ice shelf water plume

Lars H. Smedsrud[1] and Adrian Jenkins
British Antarctic Survey, Cambridge, UK

Received 11 March 2003; revised 22 October 2003; accepted 11 December 2003; published 17 March 2004.

[1] We present a model for the growth of frazil ice crystals and their accumulation as marine ice at the base of Antarctic ice shelves. The model describes the flow of buoyant water upward along the ice shelf base and includes the differential growth of a range of crystal sizes. Frazil ice formation starts when the rising plume becomes supercooled. Initially, the majority of crystals have a radius of ~0.3 mm and concentrations are below 0.1 g/L. Depending on the ice shelf slope, which controls the plume speed, frazil crystals increase in size and number. Typically, crystals up to 1.0 mm in radius are kept in suspension, and concentrations reach a maximum of 0.4 g/L. The frazil ice in suspension decreases the plume density and thus increases the plume speed. Larger crystals precipitate upward onto the ice shelf base first, with smaller crystals following as the plume slows down. In this way, marine ice is formed at rates of up to 4 m/yr in some places, consistent with areas of observed basal accumulation on Filchner-Ronne Ice Shelf. The plume continues below the ice shelf as long as it is buoyant. If the plume reaches the ice front, its rapid rise produces high supercooling and the ice crystals attain a radius of several millimeters before reaching the surface. Similar ice crystals have been trawled at depth north of Antarctic ice shelves, but otherwise no observations exist to verify these first predictions of ice crystal sizes and volumes. *INDEX TERMS:* 1827 Hydrology: Glaciology (1863); 4207 Oceanography: General: Arctic and Antarctic oceanography; 4255 Oceanography: General: Numerical modeling; 4540 Oceanography: Physical: Ice mechanics and air/sea/ice exchange processes; 4568 Oceanography: Physical: Turbulence, diffusion, and mixing processes; *KEYWORDS:* frazil ice crystals, ice shelf water, marine ice

Citation: Smedsrud, L. H., and A. Jenkins (2004), Frazil ice formation in an ice shelf water plume, *J. Geophys. Res.*, *109*, C03025, doi:10.1029/2003JC001851.

1. Introduction

[2] Approximately 60% of the ice discharge from Antarctica passes through floating ice shelves, from which it is lost by basal melting and iceberg calving. The ice shelves cover a total area as large as the Greenland Sea and range in thickness from 100 to 2000 m. Because the freezing point of seawater falls with increasing pressure, the water that flows in beneath the ice shelves is invariably warmer than the freezing point in situ. Melting at the ice-water interface cools and dilutes the seawater, creating ice shelf water (ISW), a water mass colder than the surface freezing point. The ISW is buoyant compared with the warmer, saltier inflow and thus tends to rise along the base of the ice shelf, entraining the surrounding water to some degree [*Nøst and Foldvik*, 1994]. This process drives an overturning circulation in the sub-ice shelf ocean.

[3] As the ISW rises, it becomes supercooled in situ, and formation of ice starts. Observations suggest that the ice forms as frazil ice crystals, which are initially suspended in the water column but are subsequently deposited as a slushy layer at the base of the ice shelf. Consolidation of the slush then leads to layers of solid marine ice that have been observed up to 350 m thick [*Oerter*, 1992; *Thyssen et al.*, 1992]. Some of the frazil crystals remain in suspension and are transported out from underneath the ice shelf [*Dieckmann et al.*, 1986].

[4] Frazil ice is important to the sub-ice ocean dynamics and overall glacial ice mass balance for two reasons: (1) Frazil ice growth is a more effective sink for supercooling than is the growth of columnar ice directly onto the ice shelf base, and (2) the presence of suspended ice crystals makes the ISW more buoyant. The formation of frazil thus modifies the forcing on the overturning circulation, which, in combination with the process of crystal deposition, determines the location and rate of marine ice accumulation at the ice shelf base [*Jenkins and Bombosch*, 1995].

[5] Growth of frazil ice in salt water has been studied in laboratory experiments over timescales of the order of minutes by *Tsang and Hanley* [1985]. More recently, a set of longer laboratory experiments has been conducted [*Smedsrud*, 1998, 2001]. These experiments show that supercooling reaches a maximum before efficient frazil ice formation starts. The initial growth rate of ice is high, but this partially quenches the supercooling, and subsequent frazil ice formation proceeds at a lower rate with a persistent, low level of supercooling (~0.02°C) for up to 24 hours.

[1] Now at Geophysical Institute, University of Bergen, Bergen, Norway.

0148-0227/04/2003JC001851$09.00

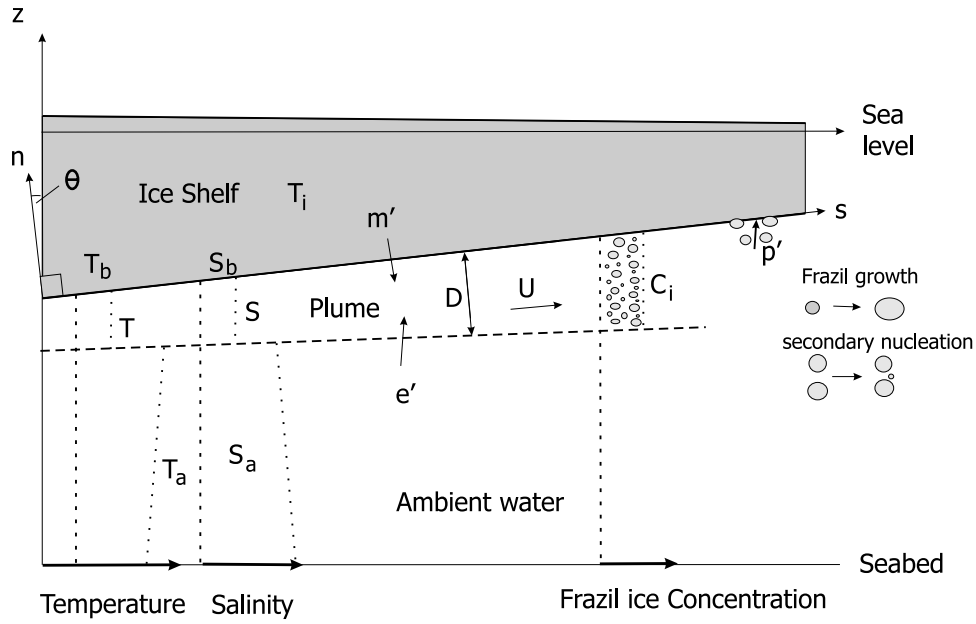

Figure 1. Sketch of the ice shelf water (ISW) plume model setup and parameters as well as the two major frazil ice processes.

This ice formation is highly dynamic, as there is a continuous increase in both the number of crystals and the individual sizes (from micrometers to ~10 mm in radius).

[6] In this paper, dynamic growth of frazil ice is incorporated into the ISW plume model of *Jenkins and Bombosch* [1995]. The following new processes are considered: (1) an evolving distribution of ice crystal sizes ranging from the micrometer to the millimeter scale, (2) differential growth and rise of ice crystals based on the crystal radius, and (3) secondary nucleation of new crystals of the smallest size. We describe the behavior of this model and how it differs from that of the earlier model of *Jenkins and Bombosch* [1995], both for an idealized, linear ice shelf base and for realistic ice thickness profiles taken from the Filchner-Ronne Ice Shelf.

2. Plume Model

[7] The plume model used here was developed by *Jenkins* [1991] as a model of the ocean beneath an Antarctic ice shelf. The model treats the ocean as a two-layer system, with the ambient water filling most of the cavity and the plume as the upper mixed layer of ISW. Tides are assumed to be a source of turbulence, which helps to keep the plume well mixed. A steady state solution for the plume is found along the (close to horizontal) ice shelf base. The plume starts at the grounding line, follows a prescribed path across the ice shelf, and ends at the ice front. The plume is characterized by a thickness D and depth-averaged values of velocity U, temperature T, and salinity S, as shown in Figure 1. The ISW plume is initiated as a small flux (0.01 m^2/s) of water at the grounding line and flows upward along the ice shelf base as a turbulent gravity current driven by its positive buoyancy, entraining ambient water along the way, as well as melting basal ice and forming new ice.

[8] Formation of frazil ice was added into the plume model by *Jenkins and Bombosch* [1995] using a single crystal size. Conservation of mass in the ISW plume takes the following forms when looking at the water fraction, the ice fraction, and the mixture, respectively:

$$\frac{\partial}{\partial s}(DU) = e' + m' + f' \tag{1}$$

$$\frac{\partial}{\partial s}[DUC_i(k)] = \frac{\rho_w}{\rho_i}[p'(k) - f'(k)] \tag{2}$$

$$\frac{\partial}{\partial s}(DU) = e' + m' + p', \tag{3}$$

where s is a coordinate that follows the ice shelf base (Figure 1). The rate of entrainment of the ambient water from below is e', and the melting and freezing at the ice-ocean interface is denoted m'. The mean reference seawater density of 1028 kg/m^3 is denoted ρ_w, and ρ_i is the constant density of (freshwater) ice of 917 kg/m^3. The frazil ice concentration $C_i(k)$ is calculated for every size class k on the basis of freezing/melting of frazil ice $f'(k)$ (section 5.3), and precipitation of frazil crystals from the plume is denoted $p'(k)$ (section 3). The terms m', f', and p' are negative when mass leaves the water fraction (freezing) or ice fraction (precipitation) of the plume, and where the dependency on size class is not explicitly written, a summation over all classes is implied. Note that a factor of $1 - C_i$ formally appears on the right-hand side of equation (1), but here, as elsewhere, it has been approximated as 1. Maximum frazil ice concentrations generated by the model are $\sim 0.2 \times 10^{-3}$ by volume, so this is a good approximation.

[9] The governing equations for momentum, heat, and salt then become

$$\frac{\partial}{\partial s}(DU^2) = D\Delta\rho g \sin\theta - C_d U\sqrt{U_T^2 + U^2} \tag{4}$$

$$\frac{\partial}{\partial s}(DUT) = e'T_a + m'T_b - \gamma_T(T - T_b) - \left(\frac{L}{C_w} - T_f\right)f' \quad (5)$$

$$\frac{\partial}{\partial s}(DUS) = e'S_a. \quad (6)$$

Equation (4) describes the water and ice mixture, while for the flux of heat and salt, equations (5) and (6) describe properties of the water phase only. The density difference $\Delta\rho$ between the plume and the ambient water is expressed by $\Delta\rho = \beta_S(\bar{S}_a - S) - \beta_T(\bar{T}_a - T) - C_i[(\rho_i - \rho_w)/\rho_w]$, where β_S and β_T are haline contraction and thermal expansion coefficients, respectively. T_a and S_a are the temperature and salinity of the ambient water below the ISW plume, while $\bar{T}_a$ and $\bar{S}_a$ are vertical averages of the ambient water over the plume depth. A dimensionless, constant drag coefficient C_d is set to 2.5×10^{-3}. The parameter g is gravity, θ is the slope of the ice shelf, and U_T is an RMS tidal current speed specified for every location along the prescribed plume track.

[10] The ice-ocean boundary temperature T_b and salinity S_b are constrained by a linear pressure freezing point relationship $T_b = aS_b + b + cz_b$, where z_b is the elevation of the ice shelf base. The coefficients a, b, and c are the slope of the liquidus (-0.0573°C per practical salinity unit (psu)), offset of the liquidus (0.0832°C), and depression of the freezing point with depth (0.761°C/km), respectively, all for seawater. The symbol γ_T denotes a heat transfer coefficient, specified in equation (10) of *Jenkins* [1991], but with U replaced by $\sqrt{U^2 + U_T^2}$, to incorporate the increased heat transfer from tidally induced turbulence at the ice-ocean interface. L is the latent heat of ice fusion, 3.35×10^5 J/kg, and C_w is the specific heat capacity of seawater, 3974 J/kg °C. The symbol T_f is the pressure freezing point at mid-depth in the plume, calculated using the plume salinity S.

3. Entrainment and Precipitation

[11] Tidal currents below Antarctic ice shelves depend to a large degree on water column thickness. *Makinson and Nicholls* [1999] found average tidal RMS speeds up to 40 cm/s below the Filchner-Ronne Ice Shelf in a barotropic model. Away from the ice front, speeds are usually in the range 2–15 cm/s, which will lead to varying current shear at the base of the ice shelf, influencing both the frictional drag and the precipitation of frazil crystals. The increased friction due to the tides is incorporated in a simple way in equation (4) by adding the tidal RMS speeds U_T.

[12] The entrainment of ambient water into the plume is parameterized as by *Jenkins* [1991] using

$$e' = E_0 U \sin\theta. \quad (7)$$

[13] Here E_0 is a dimensionless constant of 0.036. Simulations with a tidal model beneath the ice shelf indicate an upper mixed layer of ~13-m thickness using a tidal RMS velocity of 7 cm/s [*Makinson*, 2002; K. Makinson, personal communication, 2001]. This finding supports the simple parameterization of the entrainment process of equation (7) in that the tides do not increase mixing significantly beyond this depth.

[14] Precipitation of frazil crystals is modified in the same way as frictional drag by adding U_T^2 to U^2 in the approach used by *Jenkins and Bombosch* [1995]. In addition, each frazil size class has its own precipitation rate, so

$$p' = \sum_{k=1}^{N_{\text{ice}}} p'(k)$$
$$p'(k) = -\frac{\rho_i}{\rho_w} C_i(k) w_i(k) \cos\theta \left[1 - \frac{U^2 + U_T^2}{U_C(k)^2}\right]. \quad (8)$$

Precipitation starts as soon as the velocity at the base becomes lower than the critical velocity $U_C(k) = \{[0.1 g r_{ie}(k)(\rho_w - \rho_i)]/\rho_w C_d\}^{1/2}$. The model can handle an arbitrary number of frazil ice size classes N_{ice}, but 10 sizes were used as the standard, and the sensitivity to the sizes used is discussed in section 7. Here $r_{ie}(k)$ is the equivalent radius of a sphere with the same volume as the frazil disk, and $w_i(k)$ is the rise velocity of the respective frazil crystal size [*Gosink and Osterkamp*, 1983]. Precipitation occurs in only one direction, so no erosion of crystals is permitted, and $p'(k) = 0$ if $U^2 + U_T^2 > U_C(k)^2$.

4. Frazil Ice Nucleation

[15] When the ISW plume reaches its pressure freezing point, melting at the ice shelf base will cease. Shortly thereafter, the plume will become supercooled, and the heat flux will now be reversed, that is, from the ice-ocean interface downward into the plume.

[16] This situation resembles that in which platelet ice (disoriented, bladed, dendrite-like crystals) grows below thick (>1.7 m) sea ice during late winter in the Ross Sea [*Gow et al.*, 1998]. The platelet crystals can be up to 100 mm long and 50 mm wide but are more commonly around 10–20 mm, and their growth is probably due to ISW flowing beneath the sea ice cover [*Smith et al.*, 2001]. These platelet ice crystals appear to be very similar to the "large vertical crystals" observed in a core from the Ross Ice Shelf [*Zotikov et al.*, 1980]. The latter were found all the way through a 6-m-thick marine ice layer below 410 m of meteoric ice and were reported to be about 5 mm thick and 20 mm long. Platelet ice has also been observed in the lower parts of thick multiyear sea ice in the central Weddell Sea [*Gow et al.*, 1987].

[17] In the plume model it is assumed that the first growth of ice will be downward growing platelet ice as well as "normal" congelation ice. Some of the platelet ice crystals are then assumed to be broken off by turbulent eddies and will subsequently be suspended in the plume.

5. Frazil Ice Population Dynamics

[18] The frazil ice crystals are assumed to be circular disks characterized by their radius $r_i(k)$ and thickness $t_i(k)$. The size range used (r_i is between 0.01 and 4.0 mm) is similar to the range used in other numerical studies and experiments, and the approach used by *Smedsrud* [2002] is generally followed. *Smedsrud* [2002] used equations developed by *Hammar and Shen* [1995] and *Svensson and Omstedt* [1998], calibrated against experimental data on the evolution of water temperature, mean crystal diameter,

and total number of crystals. On timescales of up to 24 hours the presence of many nearby crystals effectively limits the maximum crystal size [*Forest*, 1986] and explains the maximum crystal radius of ~10 mm observed by *Smedsrud* [2001]. *Smedsrud* [2002] evaluated frazil growth over a 24-hour period, but in the ISW plume, frazil growth lasts for a number of days.

[19] The frazil disk is assumed to increase in thickness following $t_i(k) = 1/50\ 2r_i$, i.e., having a constant aspect ratio $a_r = 1/50$. This value is in the middle of the range proposed by laboratory [*Gosink and Osterkamp*, 1983] and numerical [*Jenkins and Bombosch*, 1995] experiments.

5.1. Differential Growth

[20] The heat flux from a growing ice crystal of the class k to the surrounding plume water, given in watts, is described by

$$q_i(k) = \rho_w C_w Nu K_T \frac{T_f - T}{r_i(k)} 2\pi r_i(k) t_i(k) \quad [\mathrm{W}]. \tag{9}$$

Here Nu is a Nusselt number, describing the ratio between the actual (turbulent) heat flux and the heat conduction. Nu may vary with the flow conditions and has earlier either been set of the order of 1 [*Svensson and Omstedt*, 1994] or been made a function of the turbulent dissipation rate ϵ and the Kolmogorov length scale, giving generally higher values [*Hammar and Shen*, 1995]. The molecular thermal diffusivity of seawater, K_T, is 1.4×10^{-7} m^2/s.

[21] In equation (9), no account has been made for the slower diffusivity of the salt expelled from the growing crystals. *Holland and Jenkins* [1999] show that under typical conditions the melt rate is an approximately linear function of $T_f - T$ even with this effect included. It is therefore possible to simulate the impact of salt rejection at the interface simply by reducing the effective heat transfer coefficient by a factor that varies between 1/1.6 and 1/5.7 depending on the value assumed for the haline transfer coefficient. We allow Nu to become as low as 0.2 to account for this effect here, and as discussed in section 7, this has a minor effect on the volumes of frazil formed in the plume. The radius r_i is chosen as the characteristic length scale over which the thermal gradient is estimated following *Hammar and Shen* [1995]. Our assumption that the crystals maintain a constant aspect ratio implies that two thirds of the ice growth occurs at the disk edges. We therefore use the edge area, $2\pi r_i(k) t_i(k)$, in equation (9) to estimate the rate of heat transfer between water and a growing frazil ice crystal. When frazil crystals are melting, we assume that the heat transfer takes place all over the surface, so the area of both sides of the frazil disk is added in equation (9) to yield

$$\rho_w C_w Nu K_T \frac{T_f - T}{r_i(k)} \left[2\pi r_i(k) t_i(k) + 2\pi r_i(k)^2\right].$$

[22] The frazil ice concentration in equation (2) is defined as being a volume of frazil ice suspended in a unit volume of water ΔV:

$$\begin{aligned} C_i &= \sum_{k=1}^{k=N_{\mathrm{ice}}} C_i(k) \\ C_i(k) &= \frac{1}{\Delta V} \sum_{n=1}^{N(k)} v_i(k) \end{aligned} \tag{10}$$

in m^3/m^3. Here $N(k)$ is the number of crystals in each class k, and $v_i(k)$ is the (uniform) volume of the ice crystals in that specific class, $v_i(k) = \pi r_i(k)^2 t_i(k)$. The growth rate of a frazil size class per unit volume is then

$$\frac{\Delta C_i(k)}{\Delta t} = \frac{C_w Nu K_T}{L_w} \left(T_f - T\right) \frac{2}{r_i(k)^2} C_i(k). \tag{11}$$

The growth rate $\Delta C_i(k)/\Delta t$ is calculated for each size class ($k = 1, N_{\mathrm{ice}} - 1$) and represents the growth of a constant number of ice crystals. Notice that the largest crystals ($k = N_{\mathrm{ice}}$) are not permitted to grow because they have already reached the maximum size. For melting conditions the melt rate of a frazil size class was computed in the same manner as in equation (11) with the extra surface area included, and all crystal sizes melted.

5.2. Secondary Nucleation

[23] Secondary nucleation is the term used for the production of new small crystals by removal of nuclei from the surface of parent crystals. The main processes thought to occur are collision between crystals (collision breeding) and detachment of surface irregularities by fluid shear [*Daly*, 1984]. During melting conditions the small crystals produced by secondary nucleation will soon melt away, so the process is activated in the model only during frazil ice growth. The simplified approach of *Svensson and Omstedt* [1994] is followed here.

[24] A crystal moving relative to the fluid will sweep a volume ΔV_i during a time interval Δt:

$$\Delta V_i(k) = U_r(k) \pi r_{ie}(k)^2 \Delta t, \tag{12}$$

where

$$U_r(k) = \sqrt{\frac{\epsilon}{15\nu} [2r_{ie}(k)]^2 + w_i(k)^2}, \tag{13}$$

incorporating both the rise velocity and the turbulence intensity. The dissipation rate ϵ is 7.4×10^{-6} W/kg unless otherwise stated, and the kinematic viscosity ν is 1.95×10^{-6} m^2/s. The equivalent crystal radius $r_{ie}(k)$ must be used here because the crystal can twist and turn in all directions and no method for modeling a disk in a turbulent flow has yet been formulated. The growth rate for the smallest size class resulting from collision between all the different size classes is then calculated as

$$\frac{\Delta C_i(k=1)}{\Delta t} = \sum_{k=1}^{N_{\mathrm{ice}}} \pi \bar{n}_i \frac{U_r(k)}{r_{ie}(k)} r_{ie}(k=1)^3 C_i(k), \tag{14}$$

where $\bar{n}_i$ is the average number of all the different ice crystals per unit volume in the plume. The $\Delta C_i(k = 1)$ in equation (14) is always positive (i.e., gain in ice volume), and there is a corresponding loss of (exactly the same) volume for the other classes for each part of the summation in equation (14). Several processes may limit the efficiency of the secondary nucleation process [*Smedsrud*, 2002], and $\bar{n}_i = 1.0 \times 10^3$ was found to be an empirical upper limit.

5.3. Total "Melt" Rate for Frazil Ice

[25] The ISW plume is treated as being a well-mixed upper layer, and consequently, C_i is the mean frazil ice

concentration over the plume depth D. The total rate of change of the frazil ice volume in the ISW plume in equation (5) is therefore

$$f' = \sum_{k=1}^{k=N_{\text{ice}}} f'(k) = D \sum_{k=1}^{k=N_{\text{ice}}} w'(k).$$

[26] Here $w'(k)$ is comparable with w', the rate of loss of frazil ice due to melting per unit volume of plume defined by *Jenkins and Bombosch* [1995]. Both f' and w' are negative for freezing conditions when water is lost from the plume.

[27] Because of the constant mean radius in the size classes $r_i(k)$, the actual rate of change of ice volume in one size class, $w'(k)$, depends on the melting/freezing rate $\Delta C_i(k)/\Delta t$ from equation (11) in the size below $k - 1$ and above $k + 1$. In addition, $w'(k)$ has to be consistent with a certain number of crystals being transferred to, or from, the size class. In this way the melting/freezing of all crystals in a class results in a transfer of a specific number of them to the class below/above:

$$w'(k) = \frac{1}{\Delta t}\left[\frac{\Delta C_i(k+1)}{\Delta v_i(k)} - \frac{\Delta C_i(k)}{\Delta v_i(k-1)}\right] v_i(k) \qquad (15)$$

for melting and

$$w'(k) = -\frac{1}{\Delta t}\left[\frac{\Delta C_i(k-1)}{\Delta v_i(k-1)} - \frac{\Delta C_i(k)}{\Delta v_i(k)}\right] v_i(k) \qquad (16)$$

for freezing. Here $\Delta v_i(k) = v_i(k + 1) - v_i(k)$, and equation (16) is the same as equation (18) of *Hammar and Shen* [1995]. With this formulation a class increases in volume due to melting in the class above and decreases in volume due to melting of its own crystals. In the same way a class increases in volume because of growth in the class below and decreases in volume because of growth of its own crystals. The smallest crystals ($k = 1$) have a pure loss to the class above due to growth but increase in volume because of the secondary nucleation process (equation (14)).

6. Model Behavior for a Linear Ice Shelf Base

[28] Changes in the basal slope of the ice shelf have a large impact on the behavior of a model ISW plume [*Jenkins*, 1991; *Jenkins and Bombosch*, 1995]. Therefore, in order to demonstrate more clearly the impact that the frazil ice processes described in section 5 have on the behavior of a plume, we first apply the model to an idealized ice shelf base having a constant basal slope. The early stages of the plume evolution, up to the point where the ISW becomes supercooled, are unaffected, as frazil only grows from that point onward. Following *Jenkins and Bombosch* [1995], the plume is initiated at a depth of 1400 m and ascends below a 600-km-long ice shelf, which ends at a depth of 285 m. The ambient water has linear profiles of both temperature, $T_a = -1.9°$ to -2.18°C, and salinity, $S_a = 34.5$ to 34.71 psu, from the surface to 1400 m depth. No tidal velocities are added below the linear shelf ($U_T = 0$), and the results are identical up to ~420 km and 650 m depth in all cases. Freezing processes taking place in the plume after this point will be described for the "standard run" in this section, and the sensitivity of the results to some of the key frazil ice parameters will be described in section 7. The only significant change of frazil ice parameters from *Jenkins and Bombosch* [1995] is that the crystals are assumed to be twice as thick, $t_i = a_r 2 r_i$, where $a_r = 1/50$ and not 1/100.

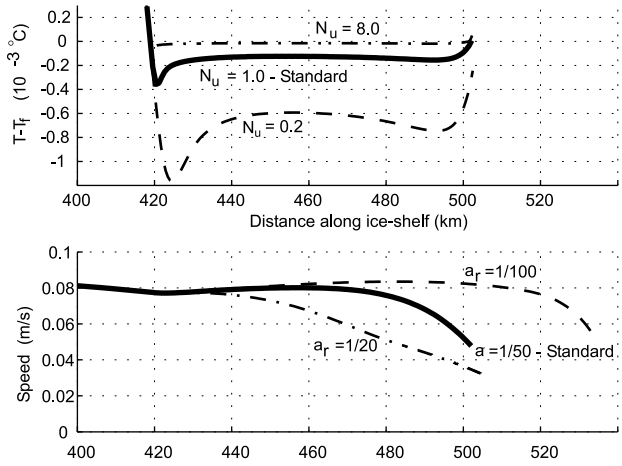

Figure 2. Supercooling ($T - T_f$) and plume speed (U) from 400 to 540 km for the linear ice shelf. The solid lines indicate standard run values. The other lines show model sensitivity.

[29] Frazil ice formation in the ISW plume takes place between 420 and 500 km. With a mean speed $\bar{U} \approx 0.05$ m/s $\approx$ 4 km/d, this distance corresponds to a time interval of about 3 weeks. Formation is initiated with a small volume of crystals ($F_0 = 40.0 \times 10^{-9}$ m^3/m^3) divided equally over the crystal spectrum. Levels of supercooling typically reach 0.2×10^{-3} °C, as shown by the solid line in Figure 2, but show no indication of oscillations like those discussed by *Jenkins and Bombosch* [1995]. The plume reaches maximum supercooling shortly after it has become supercooled, before much growth of frazil ice has taken place.

[30] The plume speed U gets a kick from the frazil ice formation, starting at 420 km (Figure 2, solid line), due to the increase in plume buoyancy caused by a positive C_i. The maximum density deficit created by frazil ice is 21.8×10^{-3} kg/m^3 when the frazil ice concentration of the plume is at its maximum, 0.18 g/L.

[31] The size spectrum for the suspended frazil ice crystals is shown in Figure 3 as a function of distance along the plume path. The radius of the frazil ice class having the largest concentration will hereinafter be called the significant frazil ice radius r_{is}. This is the radius of the class constituting the peak in the frazil ice spectrum at any given position along the plume path shown in Figure 3. At the start of the formation process, $r_{is} = 0.3$ mm. Between 460 and 490 km, r_{is} has reached 0.5 mm, and the concentration for this class is 0.07 g/L. Toward the end, r_{is} decreases again as precipitation outweighs growth for the larger classes and ends up at $r_{is} = 0.4$ mm.

[32] The supercooling in the ISW plume drives an almost constant production of frazil crystals, as shown in Figure 4. Toward the end both supercooling and crystal growth decrease. This is caused by the thickening of the plume, which tends to lower the depth-averaged freezing point used

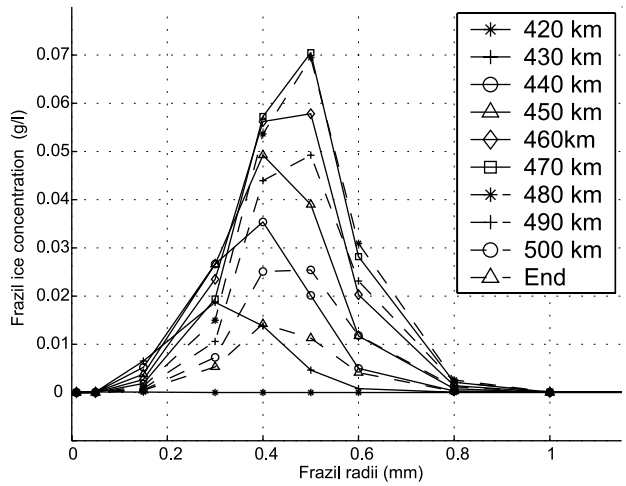

Figure 3. Frazil ice size spectrum from 420 to 509 km for the linear ice shelf.

to calculate f', as it slows down. The slightly positive values of $f'(4)$ and $f'(5)$ between 460 and 500 km are indications not of melting but of a net loss of mass to larger classes. This is caused by an ice growth in the class itself that is larger than in the class with the smaller radius that feeds it.

[33] The decrease in C_i toward the end is caused by the precipitation of the larger crystals upward onto the ice shelf base, as shown in Figure 4. Up to 470 km the precipitation comprises the 0.6- and 0.8-mm crystals, but as the plume slows down, the smaller crystals also add to the total precipitation.

[34] The plume speed and ice precipitation rate presented here are similar to the results obtained by *Jenkins and Bombosch* [1995] for crystals of 1.5 mm diameter, i.e., a frazil radius of 0.75 mm, because of the different a_r and the resulting rise velocities. The thinner 0.75-mm crystals of *Jenkins and Bombosch* [1995] have a rise velocity similar to the crystals having the significant radius of 0.5 mm found here. The evolution of T and p' differs from all the presented cases of *Jenkins and Bombosch* [1995]. In particular, there is no sign of oscillations of any kind in these parameters with the frazil spectrum included. Instead, we see a smooth return to the pressure freezing point following the initial peak in supercooling and an even distribution of p', with the largest crystals deposited before the smaller ones.

[35] The $\delta^{18}O$ values of the plume water and precipitating frazil ice have also been computed. Assuming a constant $\delta^{18}O$ in the ambient water of -0.5‰, the plume water value decreases to -0.78‰ over the first 10 km of the plume path. This decrease is due to input of meltwater from the ice shelf with $\delta^{18}O = -40$‰. Along the track, $\delta^{18}O$ increases steadily in the plume until the point of neutral buoyancy. The increase is due to entrainment of the ambient water, which dominates over further melting. When melting ends and frazil ice starts forming at 420 km, $\delta^{18}O = -0.623$‰. The supercooling of 0.2×10^{-3} °C drives an individual frazil crystal growth rate of up to 0.2 mm/h, highest for the smallest crystals. This results in $\delta^{18}O$ values for the growing frazil ice between 2.03‰ and 2.08‰, and for the larger classes, which dominate precipitation, the values are between 2.07‰ and 2.08‰. Alternatively, the fractionation for the precipitating ice is 2.695, very close to the equilibrium fractionation for sea ice of 2.7 [*Eicken*, 1998]. The frazil formation process therefore leads to $\delta^{18}O$ values similar to those produced by the growth of "normal" congelation ice directly to the ice shelf base. In both cases, equilibrium fractionation results in $\delta^{18}O$ values close to

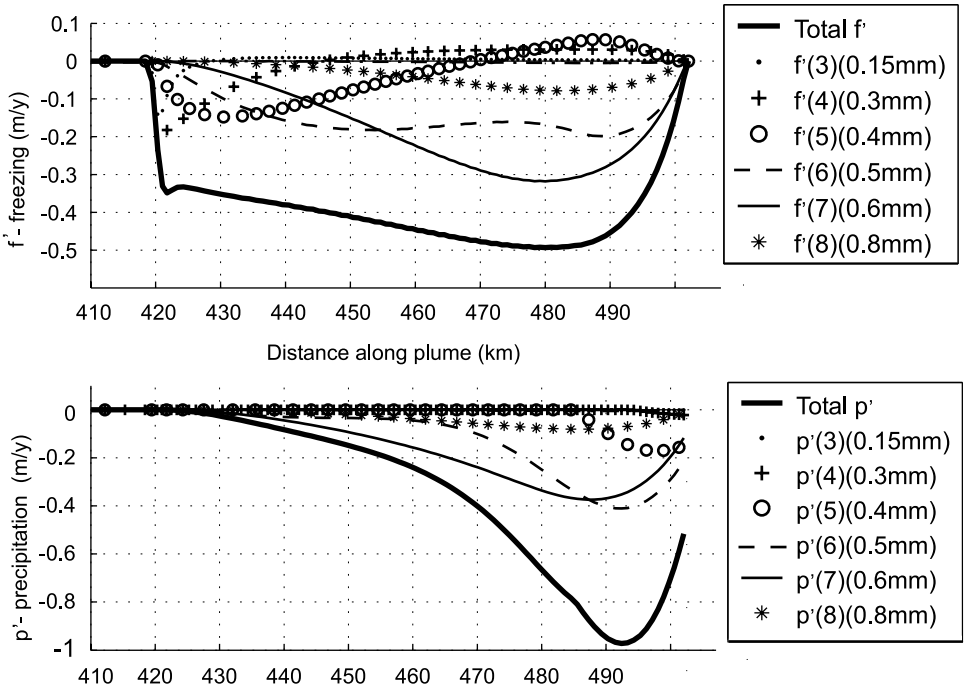

Figure 4. (top) Frazil ice growth and (bottom) precipitation for the linear ice shelf.

Table 1. Model Sensitivity to Frazil Parameters for the Linear Ice Shelf[a]

Parameter	$\bar{U}$, cm/s	$\bar{D}$, m	Maximum C_i, g/L	r_{is}, mm	Maximum $(T - T_f)$, °C	$\int_0^{end} m' ds$, m³/yr	$\int_0^{end} f' ds$, m³/yr	$\int_0^{end} p' ds$, m³/yr	End, km
Standard run	4.8	9.5	0.18	0.5	-0.35×10^{-3}	197×10^3	-33×10^3	-30×10^3	502
$Nu = 0.2$	5.1	8.5	0.17	0.5	-1.15×10^{-3}	197×10^3	-32×10^3	-30×10^3	502
$Nu = 8.0$	6.0	16.8	0.18	0.5	-0.07×10^{-3}	198×10^3	-33×10^3	-31×10^3	502
$a_r = 0.01$	5.2	11.0	0.31	0.6	-0.38×10^{-3}	193×10^3	-55×10^3	-42×10^3	533
$a_r = 0.05$	4.7	22.2	0.06	0.3	-11.69×10^{-3}	196×10^3	-21×10^3	-21×10^3	509
Low n_i	4.8	9.4	0.18	0.5	-0.35×10^{-3}	198×10^3	-33×10^3	-30×10^3	502
High n_i	5.5	15.5	0.29	0.5	-0.35×10^{-3}	193×10^3	-59×10^3	-44×10^3	537
Small seed	6.3	16.6	0.62	0.6	-0.25×10^{-3}	183×10^3	-112×10^3	-75×10^3	598
Large seed	4.6	46.3	0.03	0.6	-27.03×10^{-3}	190×10^3	-8×10^3	-8×10^3	512
Low F_0	4.6	46.3	0.03	0.6	-27.02×10^{-3}	189×10^3	-8×10^3	-8×10^3	512
Low F_0/High n_i	4.6	10.0	0.04	0.5	-0.98×10^{-3}	198×10^3	-31×10^3	-30×10^3	497
$N_{ice} = 3$	5.0	9.5	0.03	0.5	-0.6×10^{-3}	198×10^3	-30×10^3	-29×10^3	496
$N_{ice} = 25$	5.5	16.7	0.1	0.5	-0.4×10^{-3}	198×10^3	-31×10^3	-29×10^3	499

[a]The details for the different runs are given in the text, and averages and integrals are from a grounding line at 1400 m depth to the point where the plume leaves the ice shelf, given as "end." The significant frazil radius r_{is} is given at the point of maximum C_i.

2.0‰ as found in a core from the Ronne Ice Shelf [*Oerter*, 1992]. The ice formation in the plume slows the rate of increase in $\delta^{18}O$, and at 500 km $\delta^{18}O = -0.605$‰.

7. Sensitivity of Model Results to Frazil Ice Parameters

[36] Table 1 summarizes how some key model outputs change in response to varying the input parameters that define the frazil ice growth. In general, we find that the model is less sensitive to changes in the parameterization of frazil processes than was the earlier version of *Jenkins and Bombosch* [1995]. This is a result of the addition of an evolving spectrum of crystal sizes, which means that the size classes favored for growth (smaller) and precipitation (larger) either are present or can be developed.

[37] The stability of the model is well illustrated by its response to changing the Nusselt number, *Nu*, as given in Table 1. Although *Nu* analytically has a lower bound of 1.0, we use lower values here to mimic the effect of the slower (molecular) diffusion of salt, compared with heat, for the case when turbulent conditions in the plume are not fully developed. Changing *Nu* alters the supercooling of the plume as shown in Figure 2, but the crystal spectrum and the total growth and precipitation of frazil ice are nearly the same in the $Nu = 0.2$ and $Nu = 8.0$ cases. The differences in $\bar{U}$ and $\bar{D}$ are caused by the quicker start of the frazil formation process with higher *Nu*, giving a slightly higher $\bar{U}$ and thus a higher entrainment, increasing $\bar{D}$.

[38] The ease with which the ice can be retained in suspension has an important influence on model behavior. If a significant volume of frazil is suspended, then U increases and the plume stays fairly thin. The more rapid ascent of the plume increases the rate at which its pressure freezing point falls, and thus more frazil ice is produced in a feedback loop. This is illustrated by varying the crystal thickness t_i, which controls the rise velocity w_i and thus the critical velocity U_c, at which a frazil class starts to precipitate (given by equation (8)). As shown in Figure 2 and given in Table 1, a smaller t_i ($a_r = 1/100$) leads to higher U and C_i and more frazil growth. This makes the plume more buoyant, and it continues to 533 km, only depositing a portion of its suspended frazil crystals. On the other hand, thicker crystals ($a_r = 1/20$) have a larger buoyancy for any given radius and precipitate more easily. This leads to lower C_i and $\bar{U}$ and a thicker plume. The frazil spectrum is also altered, with $r_{is} = 0.3$ mm; all the crystals precipitate out at 480 km; and the total precipitation is half of that in the $a_r = 1/100$ case. The supercooling grows toward the end and reaches a high value, as there is no frazil growth after 480 km.

[39] The efficiency of the secondary nucleation process is controlled by the upper limit on $\bar{n}_i$, the average number of crystals per unit volume. In the low n_i case (Table 1) the maximum is set to one crystal, the absolute lower limit, thus effectively not permitting any secondary nucleation of new crystals. This makes hardly any difference to the results, indicating that there are enough small crystals available in the initial flux without this process and that subsequent addition of more small crystals does not alter results significantly. The high n_i case has the maximum set at $\bar{n}_i = 100 \times 10^3$ m^{-3}. This increases frazil ice production significantly and keeps the plume buoyant to 537 km.

[40] The first frazil crystals that appear in the plume are assumed to be crystals breaking off from the base, as discussed in section 5. As there are no observations to guide us toward the size of these crystals, the initial flux of frazil has been set equally between the 10 sizes used. The effect of partitioning this flux unevenly in favor of the small side of the frazil spectrum is shown in the small seed case in Table 1. The five smallest sizes have 19% of the initial flux each, while the five largest sizes have 1% each. This leads to the highest levels of frazil ice and precipitation, the highest $\bar{U}$, and a plume that stays buoyant to 598 km. The supercooling is low, as there are initially so many small crystals that can grow rapidly, and r_{is} reaches 0.6 mm as C_i keeps increasing until 580 km, when most of the crystals have attained this size.

[41] With mostly large crystals in the initial frazil flux, the large seed case in Table 1, the opposite effect is seen: less frazil ice and precipitation, a larger supercooling, and a lower $\bar{U}$. This has approximately the same effect as a lower initial flux, the low F_0 case, where $F_0 = 4.0 \times 10^{-9}$, one tenth of the standard run. The similarity is caused by the lower initial concentration of the smaller crystals in both cases.

[42] The low frazil production caused by the low F_0 can be compensated by setting the maximum $\bar{n}_i = 100 \times 10^3$,

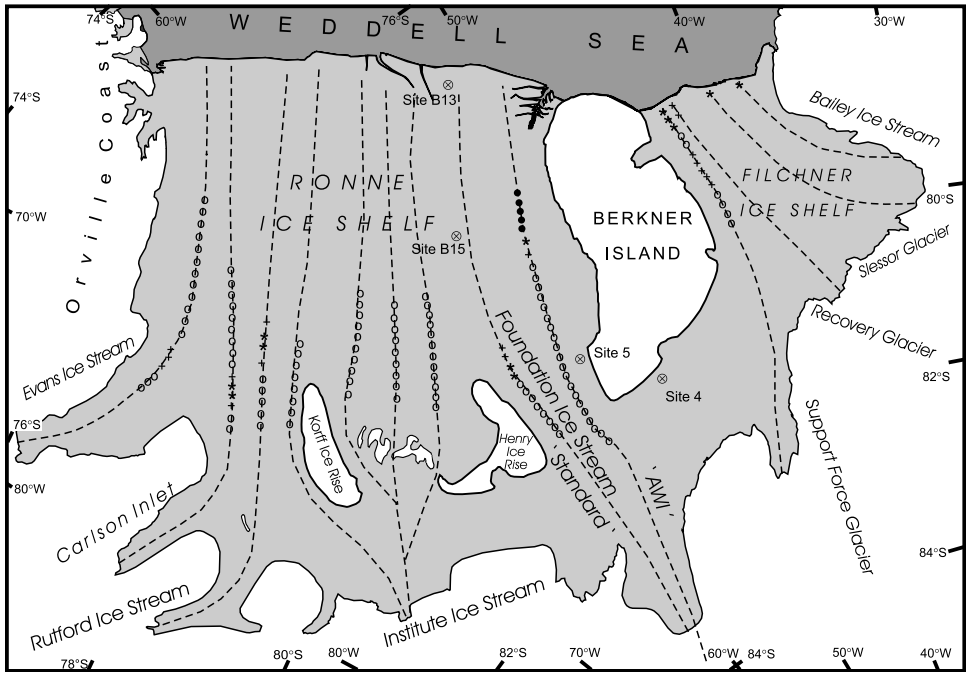

Figure 5. Map of the Filchner-Ronne Ice Shelf. The proposed plume paths illustrate results for different regions but are not predictions of ISW flow. Along the Foundation Ice Stream, there are two paths: the standard run and one farther to the east that is based on a data set from the Alfred Wegener Institute (AWI). Calculated freezing rates are indicated along the different plume paths: 0–0.5 m/yr (open circles), 0.5–1 m/yr (plus signs), 1–2 m/yr (asterisks), and >2 m/yr (solid circles). Drill sites mentioned in the text are also marked (circled crosses).

the low F_0/high n_i case. This increases frazil ice growth and precipitation back to the level of the standard run despite an overall lower ice concentration. The lower concentration promotes growth in all size classes because of the higher level of supercooling, and with a very efficient secondary nucleation process a supply of the precipitating size classes can be maintained.

[43] With equations (9)–(16) describing the frazil growth, the minimum value for $N_{\text{ice}} = 3$. Using $r_i = (0.01, 0.5, 0.8)$ mm leads to a maximum C_i of 0.03 g/L, much lower than the standard run value of 0.18 g/L (Table 1). Despite this, the total volume of frazil grown and precipitated remains almost unchanged. Once again, the higher supercooling promotes crystal growth, and with fewer size classes, frazil reaches the greatest volume (0.8 mm) faster. Precipitation therefore parallels growth and maintains the low concentration. This leads to a more evenly distributed precipitation around 0.4 m/yr between 420 and 500 km, very similar in pattern to the total f' shown in Figure 4, divided equally between the 0.5- and 0.8-mm crystals. There is a small sign of an oscillation in the temperature of the plume: first, the usual return to the (now lower) equilibrium temperature, then an increase in supercooling, resulting from the low frazil concentrations, before entrainment raises T again around 480 km. This is very similar to the form of T in the case of $Nu = 0.2$, shown in Figure 2.

[44] Increasing the number of crystal classes (N_{ice}) to 25 allows a 0.1-mm resolution in the r_i spectrum but does not alter the results significantly (Table 1). There is a slight broadening of the peak in the frazil spectrum shown in Figure 3, and the maximum C_i reaches 0.1 g/L at 454 km.

[45] Overall, we find that the most robust result is the size spectrum of suspended crystals, as characterized by r_{is}. This is a key finding, which lends us some confidence in our predictions of the crystal sizes precipitated to form marine ice. The total amount of precipitation is also a fairly robust result, although it is sensitive to the availability of small seed crystals. Unfortunately, this is the parameter we probably know least about. The result which shows most sensitivity to the choice of model parameters is the level of supercooling. However, its impact on model results is relatively small, since changes in the level of supercooling are often compensated by variations in ice concentration or plume volume flux, such that the total growth of frazil ice remains relatively stable. There is also an advantage in the high sensitivity of this variable. Salinity, temperature, and pressure are the easiest properties of all to observe beneath an ice shelf and turn out to be the most useful in helping us to narrow down the appropriate choices for our unknown model parameters.

8. Foundation Ice Stream Results

[46] The Foundation Ice Stream flows into the central area of the Filchner-Ronne Ice Shelf as shown in Figure 5. The largest body of marine ice on the ice shelf is thought to originate from water flowing approximately along the proposed standard run path [*Bombosch and Jenkins*, 1995]. We use the plume paths to represent a region of ISW flow. The plume paths in Figure 5 are not predictions of ISW flow, as there is only one horizontal coordinate in the model and no account is taken of cross-flow forces (i.e., Coriolis).

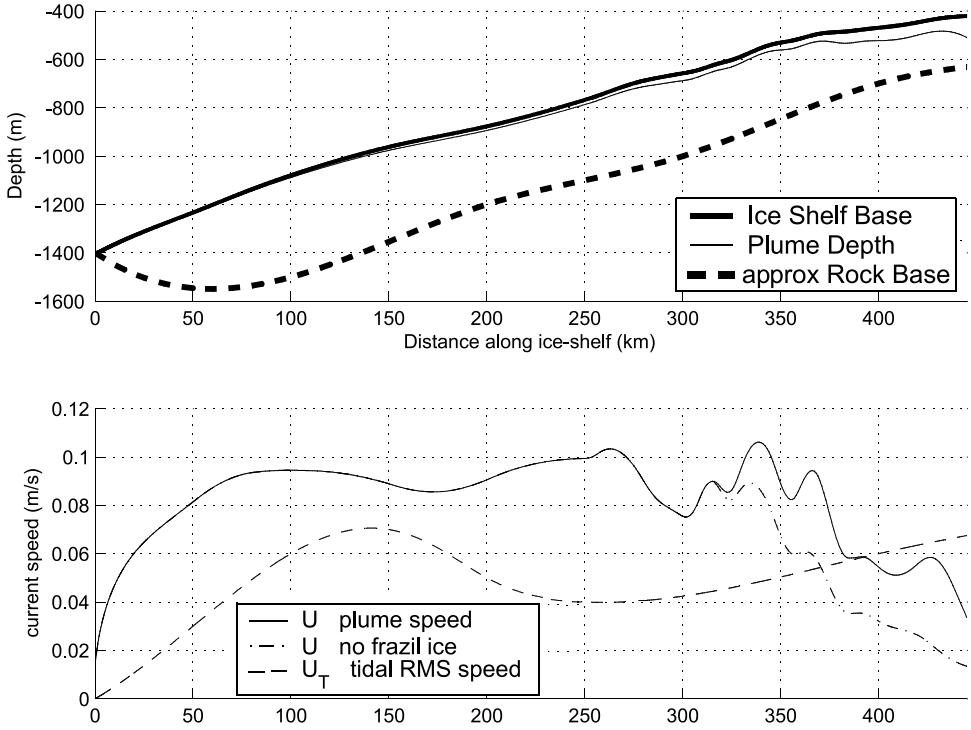

Figure 6. Along-track ice shelf and seabed topography for the Foundation Ice Stream, with (top) plume thickness and (bottom) speed of the plume U and prescribed tidal speed U_T.

We will use this section to describe model results in a natural setting, and the model's response to different forcing will be discussed in section 9. The ambient water properties are the same as for the linear ice shelf, and they have been used throughout unless otherwise stated. The properties are $T_a = -1.9°C$ and $S_a = 34.5$ psu at the surface, decreasing/increasing to $T_a = -2.18°C$ and $S_a = 34.71$ psu at 1400 m depth.

[47] The depth of the Filchner-Ronne Ice Shelf along the proposed standard run path is shown in Figure 6 together with the calculated plume depth D and a rough bottom bathymetry. The value of D increases almost linearly from 0 to 20 m over the first 250 km, then stays fairly constant around 30 m for the next 100 km before increasing to 100 m over the final 100 km. The ISW plume becomes neutrally buoyant here and leaves the ice shelf at approximately 500 m depth, with ~300 m of ambient water below.

[48] The plume speed U shown in Figure 6 is controlled largely by the slope of the ice shelf base. The variability in U between 250 and 400 km is caused by increased resolution in the ice shelf profile in this region. Up to 250 km the data on ice shelf thickness are more sparse, so basal elevation and velocity profiles appear smoother [*Lythe et al.*, 2001]. The effect of suspended frazil ice in the plume is shown by plotting U from a model run without frazil ice, where U is ~3 cm/s lower between 320 and 400 km. Prescribed U_T is also shown and has been added in both cases to the ice-ocean drag in equation (4). The main impact of this is to reduce U by ~2 cm/s in the region between 50 and 250 km, where tidal currents are high and the plume remains thin. At 370 km, C_i is at its maximum, 0.38 g/L, and this makes the plume density 45.8×10^{-3} kg/m^3 less than it would be without frazil ice. This increases U from 5.5 cm/s with no frazil to the 9 cm/s shown in Figure 6.

[49] Frazil ice starts to form when the plume becomes supercooled at 315 km, as shown in Figure 7. The rise of the plume increases T_f, and this is the source of supercooling driving the growth of frazil ice. As all the frazil crystals in the plume model experience the same supercooling, it is the smallest crystals that grow most efficiently because of the

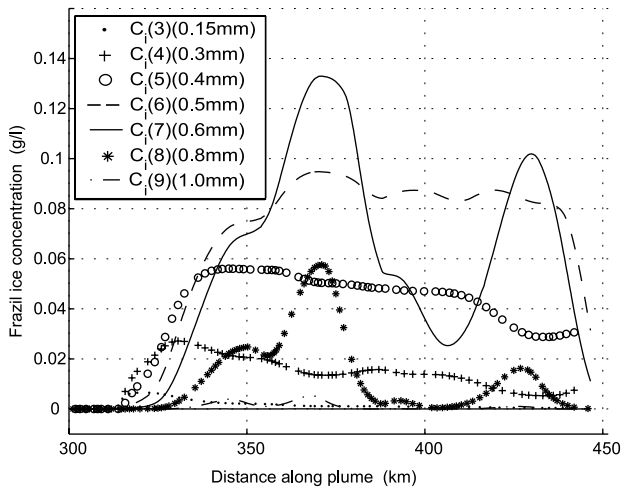

Figure 7. Frazil ice size spectrum for the Foundation Ice Stream. Size classes $C_i(1)$, $C_i(2)$, and $C_i(10)$ have concentrations too small to show on the plot.

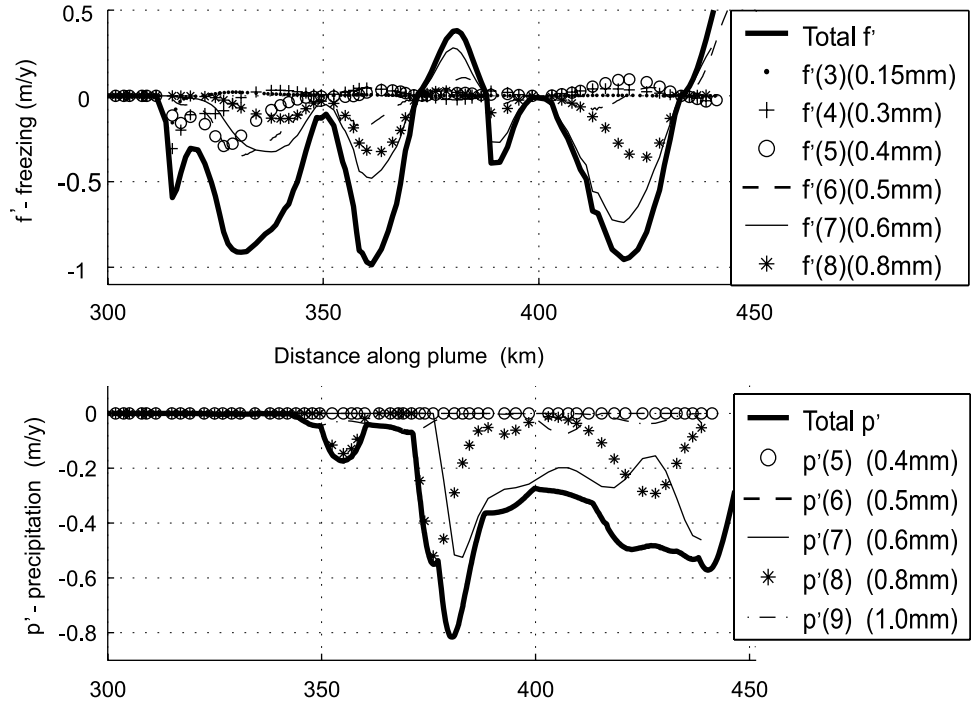

Figure 8. Freezing (negative) and melting (positive) of (top) frazil ice $f'(k)$ and (bottom) precipitation of frazil ice $p'(k)$ for the Foundation Ice Stream.

$[T - T_f]/[r_i(k)]$ term in equation (9). This also means that they leave their size class quickly, and only $C_i(3)$ to $C_i(9)$ hold enough mass to show in Figure 7. The delay before the rise in mass of each of the different classes shows clearly in Figure 7, and $C_i(9)$ is the last class to gain any significant mass around 340 km.

[50] Significant precipitation starts at 350 km, then occurs again at 370 km, with the 0.8-mm crystals, $p'(8)$, as shown in Figure 8. Thus the decreases in $C_i(8)$ in Figure 7 are caused by precipitation out of the plume. Shortly thereafter, the 0.6-mm crystals, $p'(7)$, also start to precipitate. While C_i is at its maximum, $C_i(7)$ is the class with the major ice volume; that is, r_{is} = 0.6 mm. Between 370 and 410 km, U decreases steadily, causing successive peaks for $p'(8)$ and $p'(7)$ and just a small contribution from $p'(6)$ at 405 km. There is an increase in the slope of the ice shelf around 420 km, causing a rise in U and lower $p'(7)$ and thereby an increase and second peak in $C_i(7)$ at 430 km, shown in Figure 7. After this the smaller sizes ($C_i(6)$ and $C_i(5)$) take over as the ones with the major volumes. In this way the frazil spectrum resembles the one for the linear shelf in Figure 3 with a buildup from the smaller to larger classes, precipitation, and then a shift toward smaller crystals thereafter.

[51] Melting of frazil ice (Figure 8) starts at 430 km, caused by the thickening of the plume as it slows down. This is at least partially an artifact caused by the mixed layer approach. The frazil crystals in the upper half of the plume will still be in supercooled water, and growing, while the ones in the lower part will be surrounded by water that is above the local freezing point. Because we assume that C_i is well mixed, melting dominates once supercooling is confined to less than half the plume depth. When the plume leaves the shelf at 448 km, C_i = 0.08 g/L. That is, the plume holds a total of 7.7 kg/m^2 of frazil ice in suspension.

9. Sensitivity of Foundation Ice Stream Results to Variations in Forcing

[52] Temperature and salinity data from below the Filchner-Ronne Ice Shelf have been obtained, using hot water-drilled access holes, at five sites during the 1990s [*Nicholls and Makinson*, 1998; *Nicholls et al.*, 2001]. Sites 4 and 5 were drilled at the southern tip of Berkner Island ~200 km north of the grounding line of Foundation Ice Stream (Figure 5). Properties close to the seabed at the two sites were quite similar, with a temperature close to −2.25°C and a salinity of around 34.65 psu for the bottom 200–300 m. The S4 case in Table 2 is forced with the observed temperature and salinity from site 4 as T_a and S_a between 700 m and the depth of the grounding line (1400 m). Because of the low T_a, melting is modest (up to 1.1 m/yr), and the plume reaches T_f after 190 km. Frazil ice starts to precipitate at 200 km and reaches a peak of 1 m/yr at 240 km, before the plume becomes neutrally buoyant at 246 km (800 m depth).

[53] The conductivity-temperature-depth data indicate that no water below the Filchner-Ronne Ice Shelf is warmer or saltier than Western Shelf Water (WSW) with properties $T_w \approx -1.9$°C and $S_w \approx 34.8$ psu [*Nicholls and Makinson*, 1998; *Nicholls et al.*, 2001]. This means that WSW acts as an upper boundary on the heat content and salinity of the ambient water. Tidal stirring is, in general, strong enough to promote basal melting along the Ronne ice front, cooling the inflowing WSW toward the temperatures quoted above [*Makinson*, 2002]. The WSW case in Table 2 is forced by a homogeneous ambient water column with $T_a = -1.9$°C and

Table 2. Model Response for Foundation Ice Stream

Parameter	$\bar{U}$, cm/s	$\bar{D}$, m	Maximum C_i, g/L	r_{is}, mm	Maximum $(T - T_f)$, °C	$\int_0^{\text{end}} m' ds$, m³/y	$\int_0^{\text{end}} f' ds$, m³/yr	$\int_0^{\text{end}} p' ds$, m³/yr	End, km
Standard run	7.7	23.8	0.35	0.6	-0.53×10^{-3}	216×10^3	-43×10^3	-35×10^3	446
S4	6.5	12.2	0.16	0.5	-0.33×10^{-3}	120×10^3	-23×10^3	-21×10^3	246
WSW	11.3	29.1	1.01	1.0	-59.2×10^{-3}	419×10^3	-236×10^3	-0.4×10^3	716
$U_T = 0$	8.8	20.6	0.32	0.6	-0.51×10^{-3}	236×10^3	-31×10^3	-31×10^3	423
0.5 U_T	6.3	96.3	0.33	0.6	-0.55×10^{-3}	186×10^3	-30×10^3	-30×10^3	589
2.0 U_T	6.7	24.6	0.46	0.6	-0.55×10^{-3}	166×10^3	-4×10^3	-0.5×10^3	474
$Cd = 0.25 \times 10^{-3}$	18.4	19.6	0.09	0.5	-1.23×10^{-3}	470×10^3	-71×10^3	-54×10^3	430
$Cd = 15.0 \times 10^{-3}$	2.5	49.0	0.11	0.4	-0.27×10^{-3}	59×10^3	0	0	416
AWI[a], $U_T = 0$	12.6	51.5	1.62	1.0	-0.80×10^{-3}	747×10^3	-421×10^3	-271×10^3	605
AWI	11.8	58.4	2.32	1.3	-58.6×10^{-3}	581×10^3	-1071×10^3	-109×10^3	736

[a]AWI is Alfred Wegener Institute.

S_a = 34.8 psu, representing the maximum possible heat transport to the grounding line. The warm WSW nearly doubles the total melting of the plume, and the high salinity of the upper water column means that the plume remains buoyant until it reaches the surface at the ice front. The melting peak increases from 1.65 m/yr in the standard run to 2.85 m/yr, and freezing starts at 415 km instead of 313 km.

[54] The impact of the added tidal speeds U_T in the standard run is demonstrated by comparison with a run using $U_T = 0$ throughout. In the latter case the precipitation takes place in one major event at 380 km, with a peak of 1.9 m/yr, and the plume ends at 423 km when all frazil has precipitated out. The frazil ice production is a lot higher in the standard run because of continued growth up to the end of the integration at 446 km. However, much frazil ice remains in suspension at the end point, so the difference in $\int_0^{\text{end}} p' ds$ between the two runs is only minor (Table 2).

[55] A lower tidal speed will occur during neap tides, and the effect is illustrated by setting U_T to half its value in the standard run. This leads to one precipitation event, as in the $U_T = 0$ case, but the peak is broader and reaches only 1.5 m/yr. The lower mean speed and the higher mean thickness of the plume are caused by deceleration and thickening between 400 km and the end point at 589 km. Higher tidal speeds will occur during spring tides, and with U_T set to twice its standard run value, there is hardly any precipitation at all. The total frazil growth $\int_0^{\text{end}} f' ds$, shown in Table 2, is only 10% of that in the standard run because the net frazil ice production (melting subtracted from freezing) is very low. Although frazil concentrations reach higher values than in the standard run, nearly all of the frazil ice stays in suspension and melts before the plume becomes neutrally buoyant at 474 km.

[56] The roughness of the basal ice interface is not known. Variations in the drag coefficient C_d alter the model results, most directly by slowing down or speeding up the plume. Decreasing C_d to 10% of the standard run value of $C_d = 2.5 \times 10^{-3}$ more than doubles the speed and leads to a thinner plume (Table 2). The high speed increases entrainment through equation (7) and leads to more melting of basal ice. The high speed also leads to higher supercooling as the plume ascends faster. Even though the plume becomes supercooled as late as 363 km and ends as early as 430 km in this case, more frazil has grown and precipitated because of the persistent high level of supercooling. Another effect serving to increase precipitation is the increase in the critical velocity for precipitation to occur (equation (8)); that is, decreased turbulent mixing leads to easier precipitation.

[57] Increasing C_d to 15.0×10^{-3} has the opposite effect in all respects. The plume slows down and thickens, and there is a large decrease in basal melting. Even though there is frazil growth, nothing precipitates, and all frazil melts within the plume.

[58] A new set of seabed bathymetry and ice shelf thickness data suggests that the grounding line of the Foundation Ice Stream is as deep as ~2000 m [*Lambrecht et al.*, 1999]. This data set was obtained along the path labeled AWI (Alfred Wegener Institute) in Figure 5. The deeper grounding line increases melt rates significantly as the in situ freezing point falls to −3.42°C, as opposed to −2.95°C in the standard run, and the ambient water is effectively 0.5°C warmer (AWI cases in Table 2). Without tides the basal melting peaks at 17.5 m/yr; with tides it peaks at 20 m/yr. The total melted volume is very similar between the two AWI cases. The frazil ice growth is also similar between the two AWI cases, at least up to 600 km, but without tides most of it precipitates, and with tides most of it stays in suspension.

[59] The AWI plume with tides is buoyant enough to keep going all the way to the ice front, and the frazil volumes increase to an overall maximum for all the runs on the Foundation Ice Stream. With the vertical rise at the ice front the r_{is} reaches 1.3 mm, and the largest crystals are 2 mm in radius. The total frazil growth exceeds the total melt in this case, caused mainly by T_a being set below the surface freezing point at depth. This implies that the ambient water has already been cooled by melting basal ice elsewhere on its way south before it is entrained into the plume [*Nicholls et al.*, 2001]. This south flowing current along Berkner Island may also force the proposed AWI plume path farther toward the west. An additional reason for the frazil growth to exceed total melting is the heat lost by the plume in warming the glacial ice that is melted from the ice shelf base to T_f. This is a relatively small part of the total heat budget. With the far-field temperature in the ice shelf, T_{ice}, set to −3.5°C, almost no heat goes into warming the ice, and the total melt increases by ~10% from that in the standard run. With T_i = −27°C, there is a decrease of ~8% from the standard run value.

[60] Overall, we find that the model results are most sensitive to the specification of the ambient water properties. *Lane-Serff* [1995] demonstrated that the behavior of a simple plume model was determined primarily by the

Table 3. Model Results for Freezing in the Proposed Plume Paths From West to East on the Filchner-Ronne Ice Shelf[a]

Path	Region of p', km	Minimum p', m/yr	Minimum m', m/yr	r_{is}, mm	End Depth, m	End C_i, g/L	End r_{is}, mm
Evans Ice Stream	164–245	−0.67	−0.13	0.4	−319	0.0	-
Carlson Inlet	225–308	−1.05	−0.27	0.6	−511	0.0	-
Rutford Ice Stream	321–415	−1.46	−0.16	0.6	−466	0.02	0.4
Institute Ice Stream	308–396	−0.41	−0.11	0.4	−392	0.0	-
Foundation Ice Stream	343–448	−0.82	−0.28	0.6	−420	0.08	0.5
AWI	543–652	−2.73	−0.57	1.0	0	2.32	1.3
Support Force Glacier	276–440	−0.70	−0.26	1.0	0	1.91	1.6
Recovery Glacier	303–330	−1.16	−0.08	0.6	0	1.12	1.3
Slessor Glacier	297–330	−0.16	−0.08	0.4	0	1.22	1.3
Bailey Ice Stream	243–260	−0.11	−0.10	0.3	0	1.38	1.3

[a]Region of precipitation (p') is given for values below −0.01 m/yr. The largest precipitation rate of frazil ice (minimum p') may be compared to the largest rates of basal freezing (minimum m'). The first significant frazil radius (r_{is}) is for the largest precipitation event. The draft of the ice shelf at the end of the integration is given (end depth), with the accompanying frazil concentration (end C_i) and significant frazil radius (end r_{is}).

temperature of the ambient water. In the model equations both mixing and heat transfer at the ice shelf base are linear functions of the plume velocity, and this simple proportionality lies behind the stability of the zones of melting and freezing. The relationship between plume speed and precipitation rate is nonlinear, so precipitation shows a higher sensitivity to the parameters that determine the plume velocity than is shown by either melting or direct freezing at the ice shelf base. We find that a sufficiently turbulent plume can retain all its frazil crystals in suspension, eliminating precipitation altogether.

10. Discussion

[61] As our results are predictions of the unobserved frazil crystal dimensions and concentrations that occur beneath the Filchner-Ronne Ice Shelf, results may be compared only with indirect observations. The location and rate of frazil precipitation from the modeled ISW plumes may be roughly compared with the occurrence of marine ice layers from radar sounding data [*Bombosch and Jenkins*, 1995] or freezing rates estimated from remote sensing data [*Joughin and Padman*, 2003]. Apart from this, grain sizes observed in cores of marine ice taken from the Ronne Ice Shelf can provide an absolute upper bound to the modeled frazil crystal sizes. Since grain growth will have occurred since deposition, the frazil crystals that initially settled onto the ice shelf base must have been smaller.

[62] Thin crystal plates have also been trawled from north of the Filchner Ice Shelf [*Dieckmann et al.*, 1986]. These crystals were probably flowing northward from beneath the ice shelf within a neutrally buoyant ISW plume [*Foldvik and Kvinge*, 1974] and provide the only in situ data on crystal sizes available to validate model results.

[63] The model as set up for the standard run described above has been applied to the paths shown in Figure 5. Results from these paths will be discussed in comparison with the available data.

10.1. Ronne Ice Shelf

[64] A core drilled at site B13 (Figure 5), 30 km south of the ice front, revealed evidence for a ∼90-m-thick layer of marine ice [*Eicken et al.*, 1994]. The presence of ice formed from seawater was clearly seen in the measured isotopic ratios and bulk salinities as well as in other observed properties. The grain size in the marine ice layer was found to increase with depth (and thus to decrease with age). This counterintuitive result is probably caused by sediment inclusions in the top layer that inhibit grain growth and recrystallization, and here the mean cross-sectional area of the grains was found to be ∼10 mm^2. This mean cross-sectional area corresponds to a frazil crystal radius of 1.8 mm. This is about twice the size of the largest crystals that precipitate out of the model ISW plumes. Farther down in the core the crystals have probably been able to grow freely, and the mean cross-sectional area increases to ∼30 mm^2, consistent with the estimated thermal history of the ice [*Eicken et al.*, 1994].

[65] A hot water-drilled borehole near B15 (Figure 5), about 200 km from the ice front on a flow line from the Foundation Ice Stream [*Nixdorf et al.*, 1995], showed an accumulation of unconsolidated frazil crystals, i.e., slush ice, at the ice shelf base. This confirms the presence of loose frazil ice crystals ∼80 km "downstream" of where the Foundation plume becomes neutrally buoyant in the standard run. Even though this observation is qualitative, it increases confidence in the model results.

[66] Model results for the flow of ISW beneath the Ronne Ice Shelf along the other paths shown in Figure 5 are qualitatively similar to those described in the standard run. The inclusion of a frazil spectrum tends to widen the peaks in precipitation compared with the results of *Bombosch and Jenkins* [1995], but otherwise the areas of precipitation are roughly the same, and values for the different paths are tabulated in Table 3. Tides were included for the Foundation and AWI paths. Results are similar to the freezing rates estimated from remote sensing data [*Joughin and Padman*, 2003], the only notable difference being more compact areas toward the western coasts. This difference is likely a result of the prescribed plume paths (which follow tracks along which basal elevation data are available) of the present model.

[67] The marine ice found along the Orville coast is thus fed by frazil formation in the Evans plume, and the next three plumes contribute to the marine ice west of Korff Ice Rise. Along the plume paths between Korff and Henry Ice Rises, no frazil growth is predicted, only basal freezing of 0.1 m/yr north of the rises. This suggests that the marine ice north of the rises is fed mainly by frazil formation in the Foundation plume. This is also indicated by the results of

Joughin and Padman [2003] in which the area of intense freezing to the north and west of Henry Ice Rise appears to be connected with ISW flow from the Foundation Ice Stream rather than through the gaps between Doake Ice Rumples.

[68] When tides are included for the Evans to Institute paths, overall ice concentrations increase but precipitation decreases, and the suspended frazil crystals eventually melt. This is at least partially a model artifact, as water near the ice-water interface stays supercooled, while the plume mid-depth is slightly above its pressure freezing point. Thus frazil then melts in the lower half but grows in the upper half. In reality, the frazil would tend to be more concentrated in the upper half of the plume, leading to net growth, but our simple depth-averaged equations cannot resolve such a structure.

10.2. Filchner Ice Shelf

[69] The ice crystals observed north of Filchner Ice Shelf were found at ~250 m depth [*Dieckmann et al.*, 1986]. When the ice crystals where trawled, they turned out to be thin plates (~0.5 mm thick) with rough outer edges and radii of ~10 mm. It is worth noting that the trawl net had a mesh size of 10 mm, so any crystals smaller than 5 mm in radius may have escaped the trawl.

[70] Model runs for the Filchner Ice Shelf (Figure 5) all produce a buoyant plume that reaches the ice front with frazil in suspension. The plume then rises near vertically up the ice front, the ascent from a depth of 280 m to the surface taking ~9 hours. The frazil crystal size spectrum for the Support Force Glacier plume is shown in Figure 9 and indicates that the frazil crystals grow to above 2 mm in radius, i.e., still well below the 10 mm observed by *Dieckmann et al.* [1986]. For this particular model run, T_a from *Dieckmann et al.* [1986] was used with an upper 200-m-thick layer of water ~0.1°C above T_f. Suspended frazil ice volumes increase from 1 g/L at the ice front to 1.7 g/L at the surface. Using the standard T_a, i.e., water at T_f, further increases the frazil volume at the surface (Table 3).

[71] Using a frazil ice model including a single, evolving crystal size, *Bombosch* [1998] indicated that 2.5-mm crystals could grow to a radius of 14 mm when rising 100 m at 1 cm/s in water 0.05°C below T_f. This rapid growth might be overestimated, as smaller crystals in the spectrum would tend to use most of the supercooling, inhibiting the growth rate of larger crystals. However, it is interesting to note that the high level of supercooling was actually measured at the time the crystals were trawled. The model of *Bombosch* [1998] also indicates that the crystals observed by *Dieckmann et al.* [1986] at 350-m depth melt before reaching the surface. This result follows from the assumption that the crystals rise through a passive water column. In the plume model presented here, the frazil crystals and water are assumed to move together as a bulk volume, and the crystals thus "lift" the ISW upward to the surface as in the "conditional instability" described by *Foldvik and Kvinge* [1974]. What happens in reality must be somewhere between these two extremes.

[72] Once the ISW plume has reached the surface, the integration stops, but in reality the suspended frazil crystals and plume water would separate. With the ISW losing its frazil ice, it would be 0.23 kg/m^3 denser than the surrounding water and would sink. The water remains 0.02°C supercooled, so the crystals could continue to grow while at the surface.

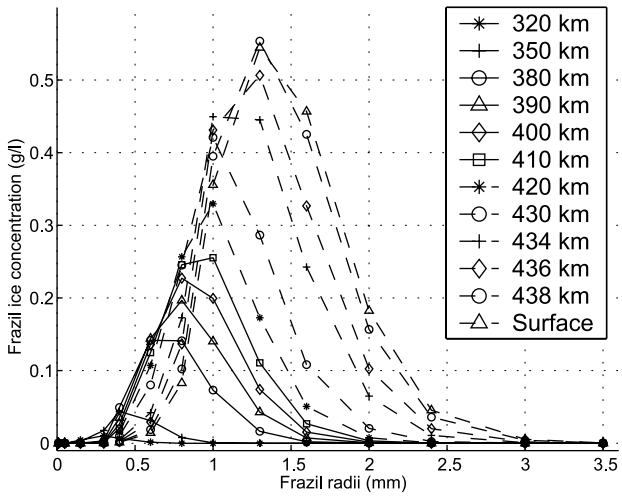

Figure 9. Frazil ice size spectrum for the Support Force Glacier ISW plume, which rises vertically at the ice front at ~430 km. Ambient temperature T_a from in situ observations is used.

[73] Precipitation in the Support Force Glacier plume (Figure 5 and Table 3) corresponds closely with the location of the 120-m-thick marine ice described by *Sandhäger* [1995]. Freezing rates estimated by *Joughin and Padman* [2003] over the same area are slightly higher. For the other plume paths on the Filchner Ice Shelf the ISW plume becomes supercooled close to the ice front, leading to small areas of precipitation as given in Table 3. All plumes reach the ice front, and the frazil-laden water rises vertically to the surface, creating high supercooling, efficient ice growth, and ice concentrations above 1 g/L (Table 3).

[74] If the vertical rise of the ISW takes place during a time when the tide is flowing south, the tidal current should prolong the rise and allow the crystal size to increase further. We cannot simulate this effect since we only add an RMS tidal current, which increases mixing but otherwise does not affect the plume evolution. Adding RMS tidal currents of ~7 cm/s to the Support Force plume only decreases precipitation to close to zero during the last 100 km.

[75] A measurement similar to the one made by *Dieckmann et al.* [1986] was made north of the Amery Ice Shelf, but in the latter case the overall mass of ice was measured [*Penrose et al.*, 1994]. The trawl had a finer mesh size of 1.5 mm, and crystals were reported to have radii in the range 5–12 mm. The mass of frazil ice divided by the trawled water volume implies concentrations between 34 and 129 $\times$ 10^{-6} g/L for the two trawls made. This is a lower estimate of the in situ frazil concentration, as no account was taken of melting as the trawl was lifted up through the 50 m of surface waters that were roughly 0.5°C above T_f.

[76] As the plume model only calculates C_i in the upper mixed layer beneath the ice shelf, it is hard to compare the measured concentrations with model results. As with the observations of *Dieckmann et al.* [1986], extremely high supercooling, in this case ~0.5°C, was recorded at the time of the trawl. Such temperatures are consistent with low

concentrations of exclusively large crystals ($r_i \geq 5.0$ mm) and suggest that conditions might be different in a lower-turbulence environment away from solid boundaries. Certainly, secondary nucleation is likely to be ineffective with crystal number concentrations of 1 m^{-3} or lower [*Penrose et al.*, 1994]. There is evidence that upwelling events such as those simulated by the model and postulated by *Foldvik and Kvinge* [1974] do indeed occur [e.g., *Fahrbach and El Naggar*, 2001], but in these cases, there are no contemporaneous measurements of ice crystal sizes.

11. Summary

[77] Our results are the first predictions of the frazil crystal dimensions and concentrations that occur beneath ice shelves. Below the Filchner-Ronne Ice Shelf, crystal radii up to 1.0 mm are suggested, although the largest proportion (by volume) of the crystals in suspension are around 0.5 mm in radius. Maximum concentrations produced in the model runs range from 0.03 to 2.3 g/L. The suspended frazil ice adds buoyancy to the ISW because the bulk density of the ice-water mixture is up to ~0.1 kg/m^3 lower than the density of the water fraction alone. This added buoyancy helps drive the sub-ice shelf circulation, increasing the speed of the outflowing ISW.

[78] The addition of the frazil crystal population dynamics has enabled us to clarify some important aspects of the behavior of a simpler model [*Jenkins and Bombosch*, 1995]. In particular, the oscillations in supercooling and ice concentration that were apparent when the earlier model was applied to an ice shelf with constant basal slope are no longer present. These oscillations were clearly artifacts of the restriction to a single crystal size. Simulated zones of accumulation are only slightly modified by the new version of the model. The reason is that the location at which the ISW plume becomes supercooled, allowing frazil growth to commence, is determined by the depth of origin of the plume and the ambient water temperature. Once frazil growth has started, the new model tends to produce broader, slightly lower peaks of precipitation than the earlier model did.

[79] In the model runs for the Filchner-Ronne Ice Shelf, significant precipitation occurs for crystals of radius 0.5–1.0 mm. After the first precipitation event, smaller crystals follow as the plume speed decreases because of the loss of buoyancy. In this way, larger crystals are deposited first, and smaller ones are deposited farther downstream. We have no observational evidence with which to verify these results. All we can say is that the minimum grain size of 1.8 mm, found in a core of marine ice extracted from Filchner-Ronne Ice Shelf [*Eicken et al.*, 1994], is consistent with crystals of these dimensions or smaller making up the initial accumulation of ice.

[80] The focusing of frazil precipitation by the dynamics of the plume is an important feature in the model. A fast flowing, highly turbulent plume can retain its entire crystal load in suspension, while a decelerating plume produces rapid precipitation as the loss of buoyancy further slows the plume in a positive feedback loop. An increase in plume speed both decreases precipitation and increases the effective cooling rate (i.e., the rate at which the pressure freezing point rises with the falling pressure), producing yet more crystals.

[81] It is not the case that crystals of sufficient size to precipitate will always develop, whatever the speed of the plume. The reason is that the secondary nucleation process ensures a continuous supply of very small seed crystals, which grow rapidly and quench the supercooling. With the level of supercooling thus limited, the growth of the largest crystals is very slow, and in a sufficiently turbulent plume, crystals that are large enough to precipitate never grow in significant numbers.

[82] Tides increase the frictional drag felt by the plume, so there is a general deceleration along the plume path. However, tides also act to keep crystals in suspension by restricting precipitation. This effect overrides the increased frictional drag in freezing areas and increases the plume buoyancy and speed. The plume then stays buoyant longer, but entrainment of warmer water eventually supplies enough heat to overcome the effective cooling caused by the plume's rise, and the frazil crystals end up melting while still in suspension.

[83] The locations and rates at which ice crystal precipitation is simulated by the model along our chosen plume paths are in reasonable agreement with the pattern of basal freezing derived by *Joughin and Padman* [2003] from remote sensing of Filchner-Ronne Ice Shelf (Table 3). However, the net melting rates produced by the individual plume models cannot be directly compared with the net melting calculated by *Joughin and Padman* [2003] for the entire ice shelf. Our plume paths all originate at the deep grounding lines of the major ice streams, where the highest melt rates are found. Between the proposed paths the ice base is shallower and the melt rates are correspondingly lower, so no simple extrapolation of our results into these regions is possible.

12. Conclusions

[84] Accumulation of marine ice beneath Antarctic ice shelves may be simulated with a relatively simple model of frazil ice growth within an ice shelf water plume. The model shows how the processes of crystal growth and deposition influence both the spectrum of crystal sizes that are held in suspension and the buoyancy and flow of the ISW. Model results of frazil crystal size and concentrations are comparable with measurements at depths north of the ice shelves.

[85] The model, with an evolving population of frazil crystal sizes, is able to reproduce the zones of basal accumulation observed on Filchner-Ronne Ice Shelf. When the frazil ice crystals reach a critical size, usually a radius of 0.8 mm, they tend to leave the ISW by precipitating upward onto the ice shelf base, thus forming marine ice. Precipitation is generally in the range 0.5–2 m/yr but can reach up to 6 m/yr under specific conditions.

[86] In general, the ISW flow is controlled by the basal slope of the ice shelf. Frazil ice formation acts as a positive feedback mechanism on the plume speed, as more crystals in suspension increase the buoyancy and hence the speed of the plume.

[87] If the ISW plume reaches the ice front, a rapid rise of the water and crystals toward the sea surface is predicted. The pressure release is then much faster than when the plume is beneath the ice shelf, and the crystals can grow to 2.5 mm in radius. When the ice-water mixture reaches the

surface, the water fraction is $\sim$0.1 kg/m^3 denser than the surrounding water. The ISW would therefore tend to sink, leaving the crystals to form a surface ice cover.

[88] The primary limitation of the current model is the greatly simplified representation of the ocean dynamics. To remove the depth averaging and the assumption of a well-mixed layer would require the inclusion of a vertical dimension in the model, while to include the effects of Earth's rotation would require an extension to two horizontal dimensions. Thus further progress in the modeling of frazil ice beneath ice shelves will require the processes described in this paper to be incorporated into more sophisticated, two- or three-dimensional ocean circulation models.

[89] **Acknowledgments.** This research has been supported through a Marie Curie Fellowship of the European Community program "Improving Human Research Potential and the Socio-economic Knowledge Base" under contract HPMF-CT-2000-01085. We are grateful to Astrid Lambrecht (Alfred Wegener Institute) for sharing the ice shelf thickness data from the Foundation Ice Stream and Keith Makinson (BAS) for suggestions and model results on the tidal velocities.

References

Bombosch, A. (1998), Interactions between floating ice platelets and ocean water in the southern Weddell Sea, in *Ocean, Ice, and Atmosphere: Interactions at the Antarctic Continental Margin*, *Antarct. Res. Ser.*, vol. 75, edited by S. S. Jacobs and R. F. Weiss, pp. 257–266, AGU, Washington, D. C.

Bombosch, A., and A. Jenkins (1995), Modeling the formation and deposition of frazil ice beneath Filchner-Ronne Ice Shelf, *J. Geophys. Res.*, *100*, 6983–6992.

Daly, S. (1984), *Frazil Ice Dynamics*, *Monogr. Ser.*, vol. 84-1, Cold Reg. Res. and Eng. Lab., Hanover, N. H.

Dieckmann, G., G. Rohardt, H. Hellmer, and J. Kipfstuhl (1986), The occurrence of ice platelets at 250 m depth near the Filchner Ice Shelf and its significance for sea ice biology, *Deep Sea Res., Part A*, *33*, 141–148.

Eicken, H. (1998), Deriving modes and rates of ice growth in the Weddell Sea from microstructural, salinity and stable-isotope data, in *Antarctic Sea Ice: Physical Processes, Interactions and Variability*, *Antarct. Res. Ser.*, vol. 74, edited by M. O. Jeffries, pp. 89–122, AGU, Washington, D. C.

Eicken, H., H. Oerter, H. Miller, W. Graf, and J. Kipfstuhl (1994), Textural characteristics and impurity content of meteoric and marine ice in the Ronne Ice Shelf, Antarctica, *J. Glaciol.*, *40*, 386–398.

Fahrbach, E., and S. El Naggar (2001), Die Expeditionen ANTARKTIS XVI/1-2 des Forschungsschiffes POLARSTERN 1998/1999, *Ber. Polarforsch.*, *380*, 177 pp.

Foldvik, A., and T. Kvinge (1974), Conditional instability of sea water at the freezing point, *Deep Sea Res. Oceanogr. Abstr.*, *21*, 169–174.

Forest, T. W. (1986), Thermodynamic stability of frazil ice crystals, paper presented at Fifth International Symposium on Offshore Mechanics and Arctic Engineering, Am. Soc. of Mech. Eng., Tokyo.

Gosink, J. P., and T. E. Osterkamp (1983), Measurements and analyses of velocity profiles and frazil ice-crystal rise velocities during periods of frazil-ice formation, *Ann. Glaciol.*, *4*, 79–84.

Gow, A. J., S. F. Ackley, K. R. Buck, and K. M. Golden (1987), Physical and structural characteristics of Weddell Sea pack ice, *Tech. Rep. 87-14*, Cold Reg. Res. and Eng. Lab., Hanover, N. H.

Gow, A. J., S. F. Ackley, J. W. Govoni, and W. F. Weeks (1998), Physical and structural properties of land-fast sea ice in McMurdo Sound, Antarctica, in *Antarctic Sea Ice: Physical Processes, Interactions and Variability*, *Antarct. Res. Ser.*, vol. 74, edited by M. O. Jeffries, pp. 355–374, AGU, Washington, D. C.

Hammar, L., and H. T. Shen (1995), Frazil evolution in channels, *J. Hydraul. Res.*, *33*, 291–306.

Holland, D. M., and A. Jenkins (1999), Modeling thermodynamic ice-ocean interactions at the base of an ice shelf, *J. Phys. Oceanogr.*, *29*, 1787–1800.

Jenkins, A. (1991), A one-dimensional model of ice shelf-ocean interaction, *J. Geophys. Res.*, *96*, 20,671–20,677.

Jenkins, A., and A. Bombosch (1995), Modeling the effects of frazil ice crystals on the dynamics and thermodynamics of the ice shelf water plumes, *J. Geophys. Res.*, *100*, 6967–6981.

Joughin, I., and L. Padman (2003), Melting and freezing beneath Filchner-Ronne Ice Shelf, Antarctica, *Geophys. Res. Lett.*, *30*(9), 1477, doi:10.1029/2003GL016941.

Lambrecht, A., C. Mayer, H. Oerter, and U. Nixdorf (1999), Investigations of the mass balance of the southeastern Ronne Ice Shelf, Antarctica, *Ann. Glaciol.*, *29*, 250–254.

Lane-Serff, G. F. (1995), On meltwater under ice shelves, *J. Geophys. Res.*, *100*, 6961–6965.

Lythe, M. B., D. G. Vaughan, and the BEDMAP Consortium (2001), BEDMAP: A new ice thickness and subglacial topographic model of Antarctica, *J. Geophys. Res.*, *106*, 11,335–11,351.

Makinson, K. (2002), Modeling tidal currents profiles and vertical mixing beneath Filchner-Ronne Ice Shelf, Antarctica, *J. Phys. Oceanogr.*, *32*, 202–215.

Makinson, K., and K. Nicholls (1999), Modeling tidal currents beneath Filchner-Ronne Ice Shelf and on the adjacent continental shelf: Their effect on mixing and transport, *J. Geophys. Res.*, *104*, 13,449–13,465.

Nicholls, K. W., and K. Makinson (1998), Ocean circulation beneath the western Ronne Ice Shelf, as derived from in situ measurements of water currents and properties, in *Ocean, Ice, and Atmosphere: Interactions at the Antarctic Continental Margin*, *Antarct. Res. Ser.*, vol. 75, edited by S. S. Jacobs and R. F. Weiss, pp. 301–318, AGU, Washington, D. C.

Nicholls, K. W., S. Østerhus, K. Makinson, and M. R. Johnson (2001), Oceanographic conditions south of Berkner Island, beneath Filchner-Ronne Ice Shelf, Antarctica, *J. Geophys. Res.*, *106*, 11,481–11,492.

Nixdorf, U., G. Rohardt, A. Lambrecht, and H. Oerter (1995), Deployment of oceanographic-glaciological strings under the Filchner-Ronne Ice Shelf, in *Filchner-Ronne Ice Shelf Programme (FRISP) Rep. 9*, edited by H. Oerter, pp. 87–90, Alfred-Wegener-Inst., Bremerhaven, Germany.

Nøst, O. A., and A. Foldvik (1994), A model of ice shelf-ocean interaction with application to the Filchner-Ronne and Ross Ice Shelves, *J. Geophys. Res.*, *99*, 14,243–14,254.

Oerter, H. (1992), Evidence for basal marine ice in the Filchner-Ronne ice shelf, *Nature*, *358*, 399–401.

Penrose, J. D., M. Conde, and T. J. Pauly (1994), Acoustic detection of ice crystals in Antarctic waters, *J. Geophys. Res.*, *99*, 12,573–12,580.

Sandhäger, H. (1995), Review of the Münster airborne radio-echo sounding-data set: Marine ice beneath Filchner-Shelfeis; bottom reflectivity and internal structures of Berkner Island, in *Filchner-Ronne Ice Shelf Programme (FRISP) Rep. 9*, edited by H. Oerter, pp. 111–114, Alfred-Wegener-Inst., Bremerhaven, Germany.

Smedsrud, L. H. (1998), Estimating aggregation between suspended sediments and frazil ice, *Geophys. Res. Lett.*, *25*(20), 3875–3878.

Smedsrud, L. H. (2001), Frazil ice entrainment of sediment: Large tank laboratory experiments, *J. Glaciol.*, *47*, 461–471.

Smedsrud, L. H. (2002), A model for entrainment of sediments into sea ice by aggregation between frazil ice crystals and sediment grains, *J. Glaciol.*, *48*, 51–61.

Smith, I., P. Langhorne, T. Haskell, H. Trodahl, R. Frew, and M. Venell (2001), Platelet ice and the land-fast sea ice of McMurdo Sound, Antarctica, *Ann. Glaciol.*, *31*, 21–27.

Svensson, U., and A. Omstedt (1994), Simulation of supercooling and size distribution in frazil ice dynamics, *Cold Reg. Sci. Technol.*, *22*, 221–233.

Svensson, U., and A. Omstedt (1998), Numerical simulations of frazil ice dynamics in the upper layers of the ocean, *Cold Reg. Sci. Technol.*, *28*, 29–44.

Thyssen, F., A. Bombosch, and H. Sandhaeger (1992), Elevation, ice thickness and structure mark maps of the central part of the Filchner-Ronne Ice Shelf, *Polarforschung*, *62*, 17–26.

Tsang, G., and T. Hanley (1985), Frazil formation in water of different salinities and supercoolings, *J. Glaciol.*, *31*, 74–85.

Zotikov, I. A., V. S. Zagorodnov, and J. V. Raikovsky (1980), Core drilling through the Ross Ice Shelf (Antarctica) confirmed basal freezing, *Science*, *207*, 1463–1465.

A. Jenkins, British Antarctic Survey, Madingley Road, High Cross, Cambridge CB3 0ET, UK. (ajen@bas.ac.uk)

L. H. Smedsrud, Geophysical Institute, University of Bergen, Allegaten 70, N-5007 Bergen, Norway. (larsh@gfi.uib.no)